European Journal of Mechanics / A Solids 67 (2018) 272–279

Contents lists available at ScienceDirect

European Journal of Mechanics / A Solids

journal homepage: www.elsevier.com/locate/ejmsol

Prediction of the mechanical behaviour of pearlitic steel based on microcompression tests, micromechanical models and homogenization approaches

Magnus Ekh[a,*], Nasim Larijani[a], Erik Dartfeldt[a], Marlene Kapp[b], Reinhard Pippan[b]

[a] Department of Industrial and Materials Science, Chalmers University of Technology, SE-412 96 Gothenburg, Sweden
[b] Erich Schmid Institute of Materials Science, Austrian Academy of Sciences, Jahnstr. 12, 8700 Leoben, Austria

ARTICLE INFO

Keywords:
Pearlitic steel
Microcompression test
Micromechanical models
Homogenization
Anisotropy

ABSTRACT

In this paper, results from microcompression tests on pearlitic steel pillars are used to determine properties of cementite and ferrite. Pillars with different orientation of the cementite lamellae have been tested to distinguish model parameters of cementite and the ferrite in two different micromechanically based models of pearlite. Both models are based on the assumption that the yielding is primarily caused by shear of the ferrite between the cementite lamellae. In the first of these models the cementite and ferrite are modelled individually. The second model is a mesomodel of a cementite lamella together with the surrounding ferrite. Based on these micromechanically based models different homogenization approaches are adopted to obtain the macroscopic behaviour of pearlitic steel. During deformation of the pearlitic steel anisotropy evolves which is assumed to be governed by the re-orientation of the cementite lamellae during the deformation. The most fundamental homogenization approach that is studied is a 3D grain structure where the fluctuating displacement field within the grain structure is solved by using Finite Element Method (FEM). The re-orientation of the cementite lamellae is governed by the deformation of the grain structure. In the investigated analytical homogenization approaches the re-orientation is assumed to follow the areal affine assumption where the normals of the cementite lamellae are convected with the macroscopic deformation gradient. Numerical results for the different models and homogenization approaches, when subjected to simple shear loading, are given and comparisons of stress–strain response are shown.

1. Introduction

Pearlitic steel is widely used in industry today due to its high strength and good ductility Raabe et al. (2010). It is used in, e.g. cable wires (bridges), cord wires (tire reinforcement) and rails. Considering its microstructure, pearlitic steel can be viewed as a metallic composite that consists of grains (colonies) with hard and brittle cementite lamellae embedded in a soft and ductile ferritic matrix as shown in Fig. 1.

In each grain the cementite lamellae have a privileged direction. After large deformations, that can be observed in applications such as in railway wheels and rails, the directions of the cementite lamellae align which results in a macroscopic anisotropic material, cf. Ivanisenko et al. (2003); Wetscher (2006).

In literature, different types of models for the macroscopic behaviour of pearlite have been proposed. These models can be either phenomenological or microstructural based. Examples of phenomenological models can be found in e.g. Bouaziz and Le Corre (2003) and Allain and Bouaziz (2008) where the hardening part of the models takes into account e.g. volume fraction of ferrite and pearlite, dislocation interaction and spacing between cementite lamellae. Regarding microstructural based models, an example can be found in Peng et al. (2002) where a model of a pearlitic colony was proposed and a self-consistent scheme was used to obtain the homogenized response of a pearlite during cyclic loading. In Terada et al. (2004) 2D finite element models of different cementite-ferrite morphologies have been studied with respect to the cyclic behaviour of the material. A comparison of a macroscopic model proposed by Bouaziz and Le Corre (2003) and a micromechanical based model was performed in Hu et al. (2006). The investigated micromechanical model is a crystal plasticity model proposed in Watte et al. (1994) where the resistance to yielding in the slip systems depends both on their relative direction to the cementite lamellae and on the lamella distance. During simulations of wire drawing the cementite lamellae are re-oriented by an areal-affine re-orientation Dafalias (2001) (denoted the March theory cf. March (1932)) and the

* Corresponding author.
E-mail address: magnus.ekh@chalmers.se (M. Ekh).

http://dx.doi.org/10.1016/j.euromechsol.2017.09.013
Received 12 June 2017; Received in revised form 25 September 2017; Accepted 26 September 2017
Available online 21 October 2017

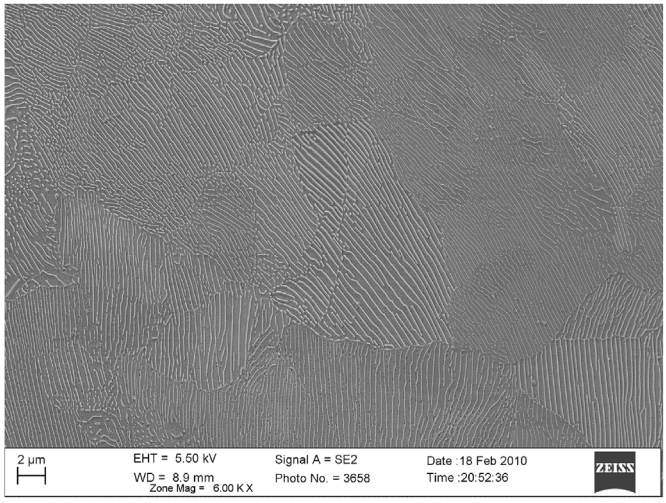

Fig. 1. Micrograph showing the microstructure of a pearlitic railway steel (900A). Image courtesy of Krste Cvetskovski.

Taylor assumption was utilized as homogenization assumption.

Another approach was utilized in Johansson and Ekh (2006) where the starting point was a micromechanical model which was then analytically homogenized using a closure assumption in order to obtain a macroscopic model taking into account re-orientation of cementite lamellae. With the same micromechanical model as a starting point, another homogenization technique was explored in Larijani et al. (2013) which relied on orientation distribution functions and integration over the surface of a unit sphere (cf. Miehe and Schotte (2004); Menzel and Waffenschmidt (2009)). Furthermore, in Lindfeldt and Ekh (2012) a micromechanical model, similar to that proposed in Peng et al. (2002), was used but the ferrite was modelled using crystal plasticity. The micromodel was used in a model for pearlitic grain structure where different prolongation conditions such as Taylor assumption, linear displacements and periodicity (see e. g Miehe et al. (1999); Kadkhodapour et al. (2011)) were used.

A limitation in the above references is that model parameters are determined from macroscopic experiments although the models are formulated based on micromechanical phenomena. The current paper starts from microcompression tests that have been conducted for pearlite with constant (or close to constant) direction of the cementite lamellae. Thereby material parameters can be fitted for the micromechanical and mesomechanical models. The micromechanical and mesomechanical models suggested in Johansson and Ekh (2006) and Lindfeldt and Ekh (2012) are chosen as prototype models. It is then shown how these models can mimic the experimental microcompression tests. Another main goal of this paper is to investigate how different homogenization assumptions influence the final response of a macroscopic experiment. This will be studied by applying simple shear loading on a pearlitic microstructure whereby the results for different homogenization assumptions in terms of stress–strain behaviour as well as cementite lamella orientation can be compared.

The paper is organized as follows: In Section 2 a large strain hyperelasticity based plasticity model is summarized which is used as a base model later in the paper. The microcompression tests on pearlitic micropillars are described in Section 3. Further, in Section 4 two micromechanical based models for a pearlitic material with a single cementite lamellae direction are introduced and adjusted to fit the microcompression tests. Different homogenization procedures to obtain the macroscopic response of a pearlite are described in Section 5. Section 6 is devoted to a numerical example of a pearlitic grain structure subjected to simple shear where results for different modelling approaches are compared. Finally, some concluding remarks are given in Section 7.

2. Elasto-plasticity model

In the current Section a standard large strain hyperelasticity based plasticity model is summarized. It will be used as a base model when defining different models for pearlite in later sections. As a point of departure, we adopt the multiplicative decomposition of the deformation gradient $\boldsymbol{F}$ into an elastic part $\boldsymbol{F}_{\mathrm{e}}$ and a plastic part $\boldsymbol{F}_{\mathrm{p}}$, i.e.

$$\boldsymbol{F} = \boldsymbol{F}_{\mathrm{e}} \cdot \boldsymbol{F}_{\mathrm{p}}. \tag{1}$$

From this decomposition a number of useful variables can be established such as the elastic Finger tensor $\boldsymbol{b}_{\mathrm{e}}$:

$$\boldsymbol{b}_{\mathrm{e}} = \boldsymbol{F}_{\mathrm{e}} \cdot \boldsymbol{F}_{\mathrm{e}}^{\mathrm{t}}. \tag{2}$$

An elastic law of neo-Hooke type is adopted such that the Kirchhoff stress can be written in terms of the elastic Finger tensor as follows:

$$\boldsymbol{\tau} = GJ_{\mathrm{e}}^{-2/3}\boldsymbol{b}_{\mathrm{e,dev}} + KJ_{\mathrm{e}}(J_{\mathrm{e}} - 1)\boldsymbol{I}, \quad \text{with } J_{\mathrm{e}} = \det(\boldsymbol{F}_{\mathrm{e}}), \tag{3}$$

where G is the shear modulus, K is the bulk modulus, and $\boldsymbol{I}$ is the 2nd order identity tensor.

The yield function is assumed to be of von Mises type and is defined in terms of the Kirchhoff stress:

$$\Phi = \sqrt{\frac{3}{2}\boldsymbol{\tau}\colon \mathbf{C}\colon \boldsymbol{\tau}} - (\kappa + Y), \tag{4}$$

where $\mathbf{C}$, in the case of isotropy, is equal to $\mathbf{I}_{\mathrm{dev}}$ which is the fourth order deviatoric projection tensor defined as , $\mathbf{I}_{\mathrm{dev}} = \boldsymbol{I} \otimes\!\!- \boldsymbol{I} - 1/3\, \boldsymbol{I} \otimes \boldsymbol{I}$[1] Y is the initial yield stress and κ is the isotropic hardening stress. It is emphasized that the current work focuses on evolution of anisotropy during monotonic loading whereby e.g. kinematic hardening is neglected. An interesting future extension of this work would be to also study cyclic loading of pearlitic micropillars.

The evolution of plasticity is assumed to be of associative type and is thereby given as (see e.g. Larijani et al. (2013)):

$$\boldsymbol{F}_{\mathrm{e}} \cdot \dot{\boldsymbol{F}}_{\mathrm{p}} \cdot \boldsymbol{F}_{\mathrm{p}}^{-1} \cdot \boldsymbol{F}_{\mathrm{e}}^{-1} = \dot{\lambda}\frac{\partial \Phi}{\partial \boldsymbol{\tau}} = \frac{3\dot{\lambda}}{2}\frac{\mathbf{C}^{\mathrm{sym}}\colon \boldsymbol{\tau}}{Y + \kappa}, \tag{5}$$

where $\mathbf{C}^{\mathrm{sym}}$ is the major-symmetrized $\mathbf{C}$, i.e. $\mathrm{C}_{ijkl} = \mathrm{C}_{klij}$. The Kuhn-Tucker loading/unloading conditions are defined as

$$\dot{\lambda} \geq 0, \quad \Phi \leq 0, \quad \dot{\lambda}\,\Phi = 0. \tag{6}$$

Finally, the evolution of isotropic hardening is assumed to be of nonlinear type:

$$\dot{\kappa} = \dot{\lambda} H \left(1 - \frac{\kappa}{\kappa_{\infty}}\right), \tag{7}$$

where H is the initial hardening modulus and κ_{∞} is the saturation hardening stress.

3. Microscopic tests of pearlite - microcompression tests

In order to find the microscopic mechanical behaviour of pearlitic steel SEM microcompression tests on pearlitic pillars have been conducted. The tests were carried out at Erich Schmid Institute of Materials Science. A fully pearlitic rail steel was deformed by high pressure torsion (HPT). The disk-shaped sample had a thickness of 5.9 mm and a diameter of 26 mm, the number of applied rotations was two and the nominal applied hydrostatic pressure was 5 GPa. The material used for the subsequent microcompression experiments in axial, tangential and inclined to axial and tangential direction was extracted at a radius r of 12 mm which correspond to an equivalent von Mises strain of approximately 15 (cf. Wetscher et al. (2007); Hohenwarter et al. (2011)). At this radius the pearlite lamellae were downscaled to a ferrite and

[1] In a Cartesian coordinate system the open products $\otimes$ and $\otimes\!\!-$ are defined as: $(\cdot \otimes \circ)_{ijkl} = (\cdot)_{ij}\,(\circ)_{kl}$ and $(\cdot \otimes\!\!- \circ)_{ijkl} = (\cdot)_{ik}\,(\circ)_{jl}$.

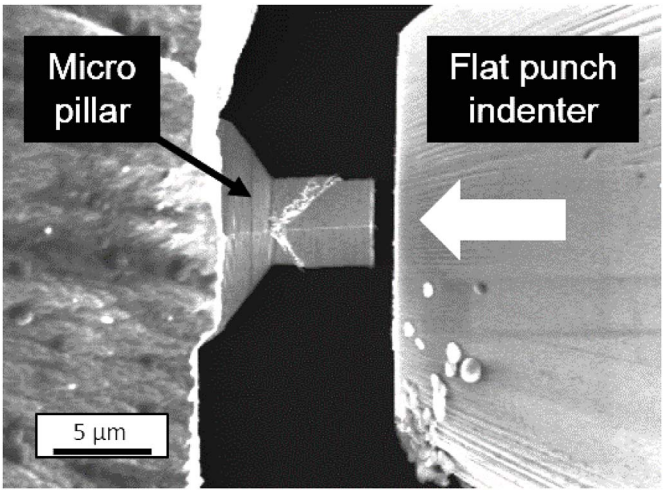

Fig. 2. A micropillar and the flat punch microindenter mounted inside a SEM.

cementite lamellae spacing of approximately 25 nm and 3 nm, respectively. Each pearlitic micropillar was milled by a focused ion beam workstation (LEO XB 1540) to dimensions of $3 \times 3 \times 6\ \mu m^3$ using a coarse milling current of 2 nA, which was followed by a polishing current of 200 pA. The micropillar is then axially loaded in compression by an electrical conductive diamond flat punch microindenter (ASMEC UNAT) mounted inside a Scanning Electron Microscope (SEM) (LEO Stereoscan 440) (see Fig. 2). The pillars are deformed in displacement controlled mode to a given displacement of $2 - 3\ \mu m$ and with a strain rate of $1 \times 10^{-3}\ s^{-1}$.

The pre-deformation in HPT causes an aligned microstructure in the samples. Therefore the pearlitic pillars can be milled so that the microstructure of the region entrapped has a certain well defined orientation. Pillars with normal, parallel and inclined orientation with respect to the loading direction were realized as illustrated in Fig. 3. Further details and discussions of the tests and their results can be found in Kapp et al. (2016).

In order to provide reliable modelling parameters the compliance of the stress–strain curve was corrected for a Young's modulus of 210 GPa in the steepest part of the unloading curve, which is not shown here. Deviations in the elastic part of the loading curves are due to a misalignment of a few nanometers between the micropillar and the flat punch microindenter and are inherent for this type of experiment. The engineering stress and engineering strain were then calculated from the force–displacement data.

4. Modelling of mesoscopic stress response

In this Section two models with the capability to predict the homogenized stress response within a microscale Representative Volume Element (RVE) are presented. The parameter values for both of the models are tuned to fit the experimental data from microcompression testing (see Section 3).

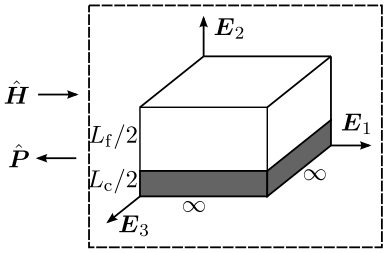

Fig. 4. Representative volume of pearlite with half a layer of ferrite ($L_f/2$) and half a layer of cementite ($L_c/2$).

It is remarked that both of the models are formulated such that they can take into account the inherent anisotropy related to the lamella structure of pearlite. This is done by formulating the models in a local microscale coordinate system $\boldsymbol{E}_i$ with a (possibly) different orientation than the macroscopic (global) coordinate system $\overline{\boldsymbol{E}}_i$. These coordinate systems are related through a coordinate transformation tensor $\boldsymbol{Q}$ such that $Q_{ij} = \boldsymbol{E}_i \cdot \overline{\boldsymbol{E}}_j$.

4.1. Model $\hat{f}_i$

A micromodel for pearlitic steel was proposed in Lindfeldt and Ekh (2012) which will be summarized in the current section. The micromodel bears resemblance to the advanced Lamel model Van Houtte et al. (2005) which is a relaxed constraint Taylor model for neighbouring grains that takes grain boundary misorientation into account.

By assuming that the planes of cementite lamellae and the ferrite have infinite width according to Fig. 4, it is possible to write the components of the deformation gradient F_{ij}' in the local Cartesian system ($\boldsymbol{E}_1$, $\boldsymbol{E}_2$, $\boldsymbol{E}_3$) as

$$F_{ij}' = \hat{F}'_{ij} + \frac{\mathrm{d}w_i}{\mathrm{d}X'_2}\delta_{j2}, \tag{8}$$

where $w_i(X'_2)$ is the components of the fluctuating displacement field and $\delta_{\circ\bullet}$ is the Kronecker's delta symbol. Furthermore, $\hat{F}'_{ij}$ are the components in the local coordinate system of the average deformation gradient acting on the micromodel. The components of the displacement gradient tensor $H'_{ij} = F'_{ij} - \delta_{ij}$ can in the same fashion be written as: $H'_{ij} = \hat{H}'_{ij} + \mathrm{d}w_i/\mathrm{d}X'_2\ \delta_{j2}$. By utilizing the fact that the micromodel is assumed to be infinite in the X'_1, X'_3-plane (and that the response is independent of X'_1, X'_3) the equilibrium equations yield that the P'_{i2} components of the first Piola-Kirchhoff stress (defined as $\boldsymbol{P} = \boldsymbol{\tau} \cdot \boldsymbol{F}^{-t}$) are constant in the whole domain. To summarize, we know that the stress components P'_{i2} and that the deformation gradient components F_{i1}' as

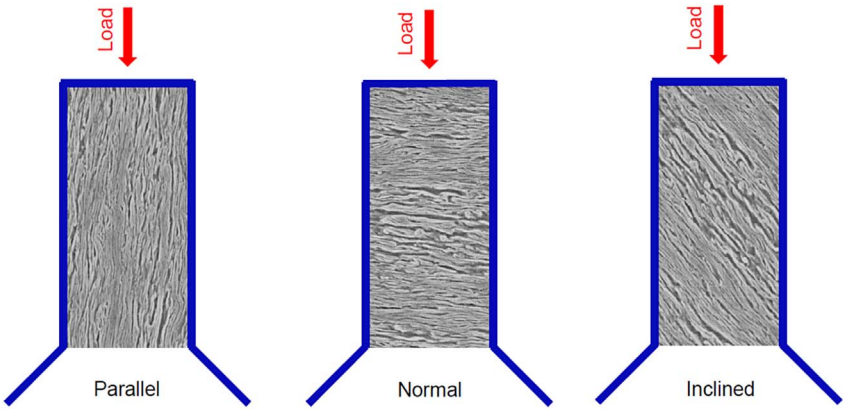

Fig. 3. A schematic of lamellae orientation in pearlitic micropillar samples with respect to the loading direction.

well as F_{i3}' are all constant in the whole micromodel. Then $\mathrm{d}w_i/\mathrm{d}X_2$ can be assumed to be constant in the ferrite and in the cementite, respectively. The fluctuation displacement therefore becomes bilinear in micromodel with the only unknowns being $w_i(L_c/2)$ i.e.

$$w_i(X_2) = \begin{cases} w_i(L_c/2)2X_2/L_c & \text{if} 0 \le X_2 \le L_c/2, \\ w_i(L_c/2)(1 - 2(X_2 - L_c/2)/L_f) & \text{elseif } L_c/2 \le X_2 \le (L_c + L_f)/2. \end{cases} \tag{9}$$

The unknowns $w_i(L_c/2)$ are solved from the equilibrium condition that P'_{i2} must be equal in the ferrite and in the cementite. The components of the homogenized 1st Piola-Kirchhoff stress $\hat{P}'_{ij}$ are obtained by volume averaging which in this case become

$$\hat{P}'_{ij} = \frac{1}{L_c + L_f}(L_c P'_{c,ij} + L_f P'_{f,ij}). \tag{10}$$

In Lindfeldt and Ekh (2012) the ferrite was modelled by using crystal plasticity whereas the cementite was assumed to behave isotropic elastic. In this paper we will focus on anisotropy evolution due to re-orientation of cementite lamellae and therefore simplify the modelling of the ferrite by adopting the isotropic elasto-plasticity model described in Section 2. The same type of model is also adopted for the cementite.

The microcompression tests described in Section 3 are used for calibration of the model. It is assumed that ferrite and cementite have the same elastic properties with Young's modulus $E = 210$ [GPa] and Possion's ratio $\nu = 0.3$. The cementite is assumed to have insignificant hardening i.e. $H = 0$. The volume fraction of cementite and ferrite is assumed to be $L_c/L_f = 0.2$. During the calibration only experimental data for the samples with inclined and the parallel orientation lamellae with respect to loading direction have been considered. Hence, the simulation for the sample with normal direction of the lamellae is a pure prediction. The objective in the calibration has been to obtain the correct saturated stress levels at $0.05 - 0.1$ strain. The results after calibration are shown in Fig. 5 and the obtained material parameters are given in Table 1.

The results for the different orientations show a relatively good agreement in the saturated stress level at $0.05 - 0.1$ strain. The simulations show geometrical hardening for larger strains which is not obtained in the experiments. It must be noted that the assumption of a uniaxial stress condition of the micropillar is a simplification whereby the true inhomogeneous 3D stress condition with e.g. strain localization cannot be captured. However, it is believed that the simplification can be used to show the capability of the model to capture the saturated stress level for different lamellae orientations.

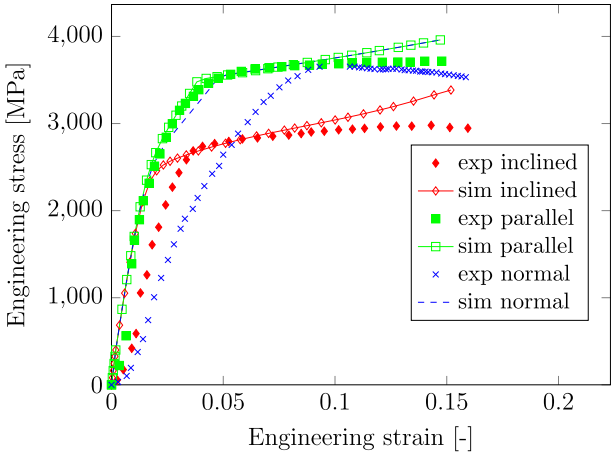

Fig. 5. Experimental and simulation results of model $\hat{f}_i$ for microcompression test.

Table 1
Material parameters for ferrite and cementite in model $\hat{f}_i$.

	E [MPa]	ν	Y [MPa]	H [MPa]	κ_∞ [MPa]
Ferrite	$210{\cdot}10^3$	0.3	400	$722{\cdot}10^3$	$1.98{\cdot}10^3$
Cementite	$210{\cdot}10^3$	0.3	8390	0	–

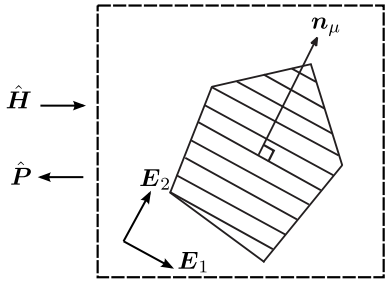

Fig. 6. A schematic of a pearlitic colony with the representative normal $\boldsymbol{n}_\mu$.

4.2. Model $\hat{f}_{i+1}$

In this section we formulate a yield function for a pearlitic colony μ with a normal $\boldsymbol{n}_\mu$ (*see* Fig. 6) as proposed and discussed in more detail in Johansson and Ekh (2006) and Larijani et al. (2013). The underlying assumption is that the plastic flow is mainly driven by shear stress (in the cementite lamellae plane) of the ferrite between the cementite lamellae. This assumption is motivated from the fact that cementite is harder than the ferrite and the elastic limit in a fully pearlitic steel is several times higher than in pure ferrite, cf. Ivanisenko et al. (2003), which was also obtained in the previous section.

The scalar shear stress measure $\hat{\tau}_\mu$ is defined as the shear component of the traction stress on the plane with the normal vector $\boldsymbol{n}_\mu$ as follows:

$$\hat{\tau}_\mu^2 = |\hat{\boldsymbol{\tau}}\cdot\boldsymbol{n}_\mu|^2 - (\hat{\boldsymbol{\tau}}\colon \boldsymbol{a}_\mu)^2, \tag{11}$$

where $\boldsymbol{a}_\mu = \boldsymbol{n}_\mu \otimes \boldsymbol{n}_\mu$. By performing some algebraic manipulations τ_μ^2 can be rewritten as

$$\hat{\tau}_\mu^2 = \hat{\boldsymbol{\tau}}\colon \mathbf{C}_\mu\colon \hat{\boldsymbol{\tau}}, \quad \text{where } \mathbf{C}_\mu = \boldsymbol{a}_\mu \underline{\otimes} \boldsymbol{I} - \boldsymbol{a}_\mu \otimes \boldsymbol{a}_\mu. \tag{12}$$

The scalar shear stress measure τ_μ can now be used to define a yield function Φ_μ according to

$$\hat{\Phi}_\mu = |\hat{\tau}_\mu| - (\hat{Y} + \hat{\kappa}), \tag{13}$$

where $\hat{Y}$ is the initial yield stress and $\hat{\kappa}$ is the hardening stress. The hardening stress is assumed to follow the evolution equation defined in Equation (7). However, yielding in the pearlitic colony does not occur only due to shear between the cementite lamellae (in the cementite lamellae plane). That would be a too restrictive deformation mode since the ferrite between the cementite lamellae has finite thickness. Furthermore, for sufficiently large stresses also cementite can yield. Therefore, the yield function is extended by a von Mises term:

$$\hat{\Phi} = \sqrt{\frac{3}{2}\hat{\boldsymbol{\tau}}\colon \mathbf{C}\colon \hat{\boldsymbol{\tau}}} - (\hat{Y} + \hat{\kappa}), \quad \text{with } \mathbf{C} = \zeta\frac{2}{3}\mathbf{C}_\mu + (1-\zeta)\mathbf{I}_{\text{dev}}, \tag{14}$$

where $\zeta \in [0,1]$ is a model parameter. During deformation the cementite lamellae will re-orient. This re-orientation is assumed to be of areal-affine type:

$$\boldsymbol{n}_\mu = \frac{\hat{\boldsymbol{F}}^{-t}\cdot\boldsymbol{n}_\mu^0}{|\hat{\boldsymbol{F}}^{-t}\cdot\boldsymbol{n}_\mu^0|}. \tag{15}$$

where $\boldsymbol{n}_\mu^0$ is the normal of the cementite lamellae before deformation. This assumption is adopted in order to ensure that $\boldsymbol{n}_\mu$ remains orthogonal to all vectors in the cementite lamella plane (since shear stress $\hat{\tau}_\mu$ in a lamella plane is computed according to equation (11)).

The material parameters are identified from the microcompression

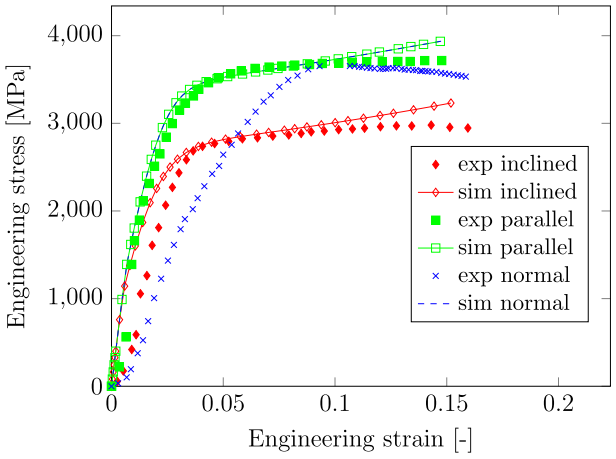

Fig. 7. Experimental and simulation results of model $\hat{f}_{i+1}$ for microcompression test.

Table 2
Material parameters of pearlitic colony in model $\hat{f}_{i+1}$.

E [MPa]	ν	$\hat{Y}$ [MPa]	H [MPa]	κ_∞ [MPa]	ζ
$210{\cdot}10^3$	0.3	719	$103{\cdot}10^3$	$1.14{\cdot}10^3$	0.69

tests. The same procedure has been followed as for model $\hat{f}_i$. The results are shown in Fig. 7 and the obtained material parameters are given in Table 2.

Even for this model, the results of the saturated stress level at $0.05 - 0.1$ strain are in rather good agreement with the experiments. The difference is that this model gives the same response for the normal and parallel directed cementite lamellae.

5. Modelling of macroscopic stress response

Two different models for a single colony $\hat{f}_i$ and $\hat{f}_{i+1}$ were proposed and discussed in Section 4.1 and 4.2, respectively. To extend the modelling to a pearlitic grain structure with randomly oriented colonies two types of models for the macroscopic response will be presented. Each integration point in these models is linked to either $\hat{f}_i$ or $\hat{f}_{i+1}$ via a transformation tensor $\boldsymbol{Q}$.

5.1. Macroscopic model based on idealization of grain structure using 3D Voronoi diagram

A 3D Voronoi diagram is generated in the free (open source) software package Neper, cf. Quey et al. (2011) and is used as an idealized representation of the grain structure, see Fig. 8.

Each of these grains has a certain lamellae orientation and is linked to either $\hat{f}_i$ or $\hat{f}_{i+1}$ (see Sections 4.1 and 4.2).

The orientation of each grain is parametrized using the two Euler angles φ and θ (see Fig. 9) such that the transformation matrix Q_{ij} (defined in Section 4) becomes:

$$Q_{ij} = \begin{bmatrix} -\sin(\varphi) & \cos(\varphi) & 0 \\ \cos(\varphi)\sin(\theta) & \sin(\varphi)\sin(\theta) & \cos(\theta) \\ \cos(\varphi)\cos(\theta) & \sin(\varphi)\cos(\theta) & -\sin(\theta) \end{bmatrix}. \tag{16}$$

The macroscopic state of deformation is imposed onto the grain structure model by restricting the fluctuation field

$$\hat{\boldsymbol{w}} = [\hat{\boldsymbol{x}} - \hat{\boldsymbol{x}}_R] - \overline{\boldsymbol{H}}\cdot[\hat{\boldsymbol{X}} - \hat{\boldsymbol{X}}_R], \tag{17}$$

where $\overline{\boldsymbol{H}}$ is the macroscopic displacement gradient and $\hat{\boldsymbol{X}}_R$ is a reference point located on the surface of the meso-RVE. The fluctuation field must be such that the volume average of the mesoscale

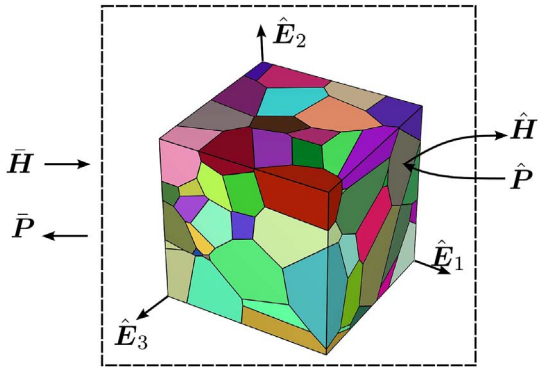

Fig. 8. 3D pearlitic model $\hat{\Omega}$ with colonies shown in different colours. (For interpretation of the references to colour in this figure legend, the reader is referred to the web version of this article.)

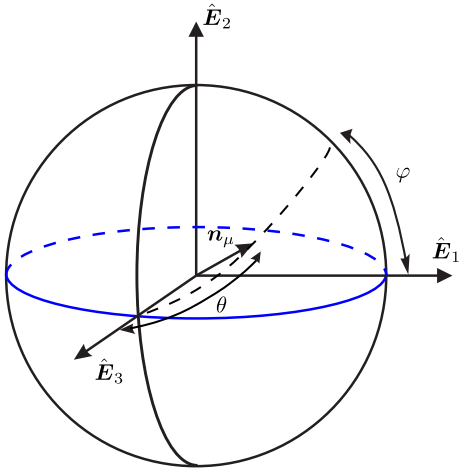

Fig. 9. Euler angles and the unit sphere.

displacement gradient within the RVE should equal the macroscopic displacement gradient:

$$\overline{\boldsymbol{H}} = \langle \hat{\boldsymbol{H}} \rangle_{\hat{\Omega}} = \frac{1}{|\hat{\Omega}|}\int_{\hat{\Omega}} \hat{\boldsymbol{H}}\,\mathrm{d}V. \tag{18}$$

Two types of prolongation assumptions on the fluctuation field $\hat{\boldsymbol{w}}$ that fulfil this condition will be exploited in the current paper:

- Taylor assumption: $\hat{\boldsymbol{w}}(\hat{\boldsymbol{X}}) = 0 \;\forall\; \hat{\boldsymbol{X}} \in \hat{\Omega}$, this means that the displacement gradient is constant in the RVE,
- Dirichlet boundary condition: $\hat{\boldsymbol{w}}(\hat{\boldsymbol{X}}) = 0 \;\forall\; \hat{\boldsymbol{X}} \in \partial\hat{\Omega}$, this means that the fluctuation of the displacements are zero on the boundary of the RVE and is solved from the equilibrium equations by using e.g. the finite element method.

For both considered prolongation assumptions the macroscopic Piola-Kirchhoff stress $\overline{\boldsymbol{P}}$ is computed as:

$$\overline{\boldsymbol{P}} = \langle \hat{\boldsymbol{P}} \rangle_{\hat{\Omega}} = \frac{1}{|\hat{\Omega}|}\int_{\hat{\Omega}} \hat{\boldsymbol{P}}\,\mathrm{d}V. \tag{19}$$

5.2. Macro-homogenization of yield function with areal affine reorientation

A hybrid micro-macromechanical model for pearlitic steel was proposed in Larijani et al. (2013). In the current section, highlights of the model and the corresponding homogenization technique are presented. The hybrid micro-macromechanical model is based on the mesoscopic model $\hat{f}_{i+1}$ presented in Section 4.2. The two main

assumptions in that model are the yield function in Equation (14) and the areal affine re-orientation defined in Equation (15). The mesoscopic yield function motivates the following expression for the macroscopic yield function $\overline{\Phi}$:

$$\overline{\Phi} = \sqrt{\frac{3}{2}\overline{\boldsymbol{\tau}}:\overline{\mathbf{C}}:\overline{\boldsymbol{\tau}}} - (\overline{Y} + \overline{\kappa}) \quad \text{with } \overline{\mathbf{C}} = \zeta\frac{2}{3}\left(\langle \boldsymbol{a}_\mu\rangle_{\hat{\Omega}} \underline{\otimes} \boldsymbol{I} - \langle \boldsymbol{a}_\mu \otimes \boldsymbol{a}_\mu\rangle_{\hat{\Omega}}\right) + (1-\zeta)\mathbf{I}_{\text{dev}}. \tag{20}$$

The re-orientation is approximated using the Taylor assumption, i.e. the deformation gradient is constant $\hat{\boldsymbol{F}} = \overline{\boldsymbol{F}}$ in the whole domain whereby:

$$\boldsymbol{n}_\mu = \frac{\overline{\boldsymbol{F}}^{-t}\cdot\boldsymbol{n}_\mu^0}{|\overline{\boldsymbol{F}}^{-t}\cdot\boldsymbol{n}_\mu^0|}. \tag{21}$$

The possible orientations for the cementite lamellae within the pearlitic microstructure in the 3D space can be represented by normal vectors pointing at the surface of a unit sphere (see Fig. 9). The homogenized stress measures are therefore obtained by averaging the corresponding stress measures on the microscopic length scale over the surface of a unit sphere. Thereby, the operator $\langle\bullet\rangle_{\hat{\Omega}}$ is defined for this type of homogenization, using the Euler angles φ and θ (see Fig. 9), as follows

$$\langle\bullet\rangle_{\hat{\Omega}} \doteq \frac{1}{4\pi}\int_0^\pi\int_0^{2\pi} \bullet \sin(\theta)\mathrm{d}\varphi\mathrm{d}\theta. \tag{22}$$

Benefiting from the *head-to-tail symmetry* of the structural tensors $\langle \boldsymbol{a}_\mu\rangle_{\hat{\Omega}}$ and $\langle \boldsymbol{a}_\mu \otimes \boldsymbol{a}_\mu\rangle_{\hat{\Omega}}$ they can be computed as follows:

$$\langle \boldsymbol{a}_\mu\rangle_{\hat{\Omega}} = \frac{1}{2\pi}\int_0^{\pi/2}\int_0^{2\pi} \boldsymbol{a}_\mu \sin(\theta)\mathrm{d}\varphi\mathrm{d}\theta, \tag{23}$$

$$\langle \boldsymbol{a}_\mu \otimes \boldsymbol{a}_\mu\rangle_{\hat{\Omega}} = \frac{1}{2\pi}\int_0^{\pi/2}\int_0^{2\pi} \boldsymbol{a}_\mu \otimes \boldsymbol{a}_\mu \sin(\theta)\mathrm{d}\varphi\mathrm{d}\theta. \tag{24}$$

The integrals are calculated numerically considering a uniform distribution of integration points over the spherical surface according to the method suggested in Bažant (1986) using 2×21 integration points.

The material parameters are macroscopic counterparts of the parameters in the pearlitic mesomodel $\hat{f}_{i+1}$. However, as an approximation the material parameter values obtained through calibration on the mesoscale (presented in Table 2) are also adopted for this model.

6. Numerical examples

By combining the two considered prolongation assumptions (see Subsection 5.1) and the two different mesomodels, four different macroscopic models are obtained. The notations used for these four models together with the hybrid micro-macromechanical model are presented in Table 3.

6.1. Characterization of anisotropy

As stated in Section 4, the two models for the mesoscopic stress response are anisotropic by construction. In this numerical example the response due to a simple shear type of loading

Table 3
Summary of macroscopic models.

Macromodel	Prolongation assumption	Mesomodel
$\overline{f}_i^{(T)}$	Taylor	$\hat{f}_i$
$\overline{f}_{i+1}^{(T)}$	Taylor	$\hat{f}_{i+1}$
$\overline{f}_i^{(D)}$	Dirichlet	$\hat{f}_i$
$\overline{f}_{i+1}^{(D)}$	Dirichlet	$\hat{f}_{i+1}$
$\overline{f}_{i+1}^{(H)}$	–	$\hat{f}_{i+1}$

$$\hat{\boldsymbol{H}} = \lambda\bar{\boldsymbol{e}}_1 \otimes \overline{\boldsymbol{E}}_2 \text{ where } \lambda \in [0,2], \tag{25}$$

is investigated as a function of the morphological orientation described by the Euler angles φ and θ (see in Fig. 9). It is remarked that the loading parameter λ is defined with respect to the global (macroscopic) coordinate system. The mesoscopic response at $\lambda = 2$ in terms of $\hat{P}_{12} = \overline{\boldsymbol{E}}_1\cdot\hat{\boldsymbol{P}}\cdot\overline{\boldsymbol{E}}_2$ is plotted in Fig. 10. From this figure it is noted that the responses from the two mesoscopic models are similar in character. The model $\hat{f}_i$ gives a slightly stiffer response, for the considered load case.

6.2. Prediction of simple shear

The 3D pearlitic model is deformed in simple shear for the models: $\overline{f}_i^{(T)}$, $\overline{f}_{i+1}^{(T)}$, $\overline{f}_i^{(D)}$ and $\overline{f}_{i+1}^{(D)}$. For simple shear the macroscopic displacement gradient is prescribed as

$$\overline{\boldsymbol{H}} = \lambda\bar{\boldsymbol{e}}_1 \otimes \overline{\boldsymbol{E}}_2 \text{ where } \lambda \in [0,2]. \tag{26}$$

By adopting Dirichlet boundary conditions (for $\overline{f}_i^{(D)}$ and $\overline{f}_{i+1}^{(D)}$) $\overline{\boldsymbol{H}}$ is applied over the boundaries of the 3D pearlitic model that consists of 625 colonies. These simulations are carried out in the commercial FE package ABAQUS and the material models are implemented as user material subroutines (UMAT). The stress distributions obtained for the 3D pearlitic models are shown in Figs. 11 and 12. The mesh consists of 65 570 elements of 4-node linear tetrahedron (C3D4) type. It is also noted here that model $\overline{f}_i^{(D)}$ gives slightly higher stresses as compared to $\overline{f}_{i+1}^{(D)}$.

The obtained macroscopic stress responses for the five models summarized in Table 3 are compared in Fig. 13. The results for stress component $\overline{P}_{12}$ in Fig. 13 show no difference between Taylor and Dirichlet prolongation conditions. The closest response to $\overline{f}_{i+1}^{(H)}$ is for model $\hat{f}_{i+1}$. It should be noted that the hybrid model $\overline{f}_{i+1}^{(H)}$ has by far the shortest computational time among the models. This together with that it shows similar qualitative response as the other more complex models, indicates that it is a good macroscopic model for pearlite subjected to large deformations and evolving anisotropy.

6.3. Convergence analysis

In this subsection the output from macroscopic models $\overline{f}_i^{T}$, $\overline{f}_{i+1}^{T}$, $\overline{f}_i^{D}$ and $\overline{f}_{i+1}^{D}$ are studied as a function of the number of colonies (i.e. the number of cementite orientations). The considered load case here is also simple shear. The obtained macroscopic response in terms of $\overline{P}_{12} = \overline{\boldsymbol{E}}_1\cdot\overline{\boldsymbol{P}}\cdot\overline{\boldsymbol{E}}_2$ is shown in Fig. 14. It is noted from these results that the macroscopic response converges already for a rather modest number of orientations.

7. Concluding remarks

The overall objective of the paper has been to show how experimental information on the microscale can be used to predict macroscopic behaviour by adopting different mesomodels for the ferrite and cementite structure together with different homogenization approaches. A particular goal has been to investigate how the choice of mesomodel and homogenization approach influences the macroscopic response.

To this end, numerical results of the mechanical behaviour of a 3D structure of pearlite have been shown for various homogenization approaches. The results in terms of homogenized stress–strain curves for simple shear loading show that the Taylor assumption gives a very similar response compared to when a fluctuating displacement field is allowed. This is particularly true for the shear stress component that is energy conjugated to the controlled shear displacement gradient. However, the information about how local stresses and strains vary within the colonies is only possible to obtain when allowing for fluctuating displacements. The fluctuating displacement field has been

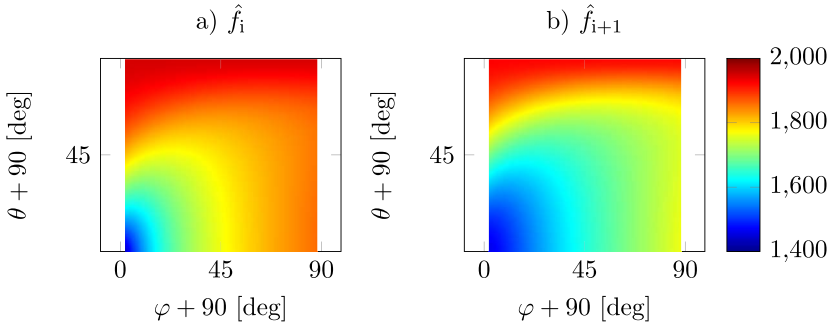

Fig. 10. Stress response in terms of $\hat{P}_{12}$ [MPa] plotted as function of the morphological angles evaluated at $\lambda = 2$ for the two mesomodels.

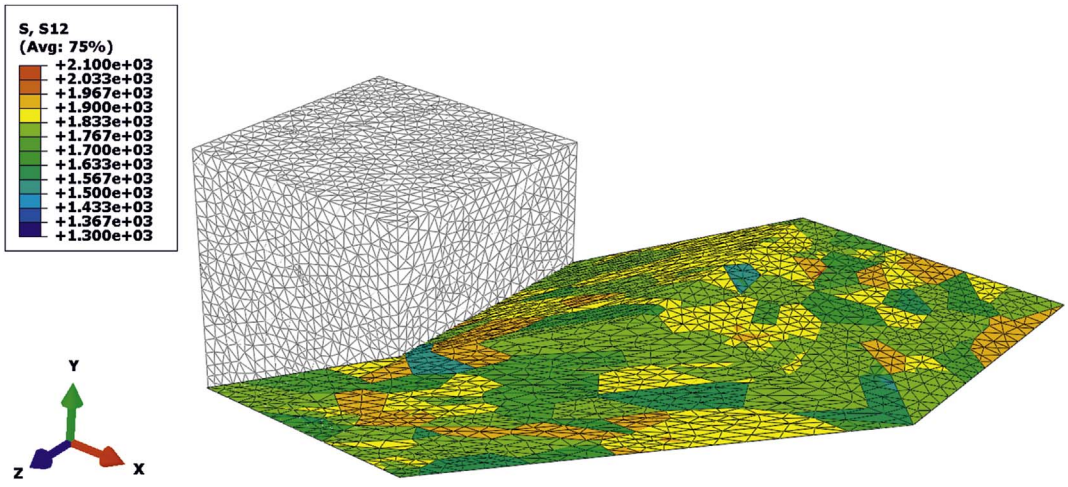

Fig. 11. Stress distribution (σ_{12} [MPa]) over the 3D pearlitic model using mesomodel $\overline{f}_i^{(D)}$ after deformation in simple shear with $\lambda = 2$ adopting Dirichlet boundary conditions.

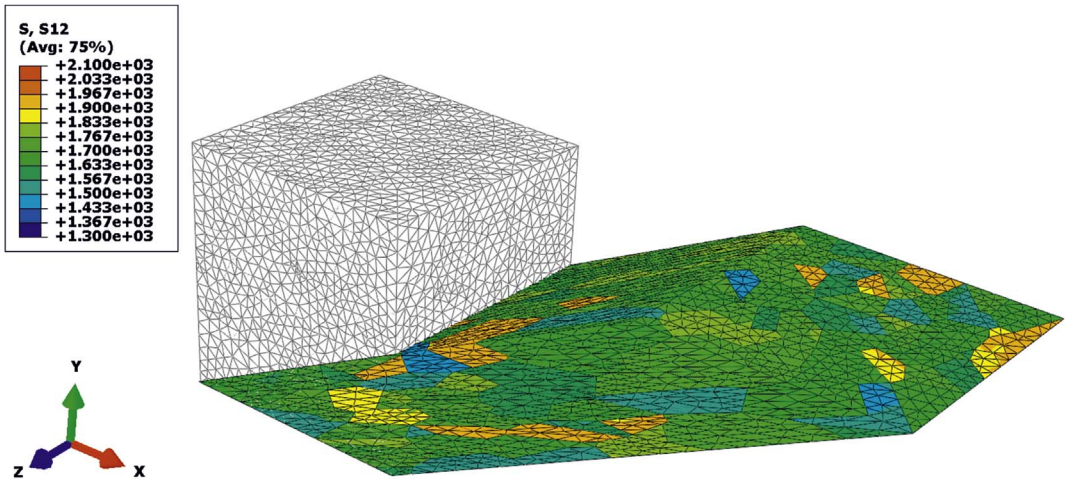

Fig. 12. Stress distribution (σ_{12} [MPa]) over the 3D pearlitic model using mesomodel $\overline{f}_{i+1}^{(D)}$ after deformation in simple shear with $\lambda = 2$ adopting Dirichlet boundary conditions.

solved using FEM and Dirichlet boundary conditions. The number of colonies (grains) with individual cementite lamellae orientation was set to 625. Two types of mesomodels were adopted in this work. However, similar conclusions could be drawn for both mesomodels. Incorporating the effect of changes in lamellar spacing in the hardening mechanisms can be considered as a future improvement in both of the mesomodels. This is of particular importance when modelling large strains. Another important issue for future work is to take into account the crystallographic texture in the ferrite by adopting a crystal plasticity model see e.g. Van Houtte et al. (2005); Lindfeldt and Ekh (2012). However, the good agreement with experimental results for saturated stress levels of normal and parallel lamellae shown in Figs. 5 and 7 indicate that the impact of crystal orientation is less important than the lamellae direction, see Kapp et al. (2016) for a more detailed discussion.

The hybrid model, which is based on simplified homogenization assumptions together with integration on a unit sphere, also gave qualitatively similar response for simple shear loading as with the Taylor assumption and with fluctuating displacements. Although the stress level was a bit lower compared to the other models. However, the hybrid model's computational efficiency as compared to the other models shows that it can be regarded as a very useful material model for pearlite subjected to large strains.

The two mesomodels that were adopted for the 3D pearlite structure were tuned to fit the saturated stress level for microcompression tests.

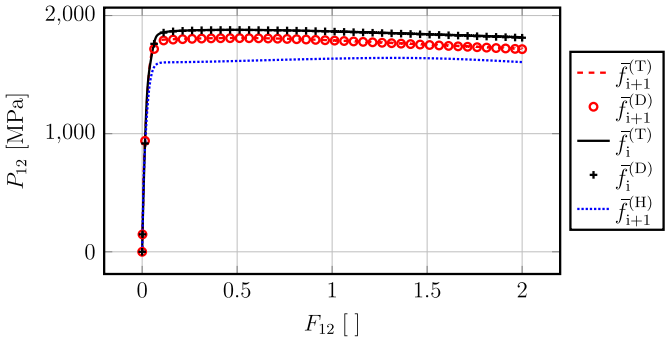

Fig. 13. Macroscopic stress response in terms of $\bar{P}_{12}$ [MPa] due to simple shear loading for the different models.

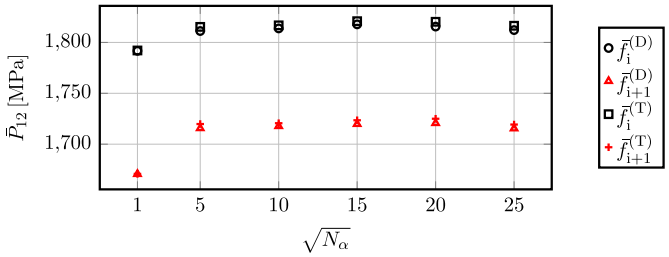

Fig. 14. Macroscopic response in terms of $\bar{P}_{12}$ [MPa] for the different models.

Both models could capture and predict the dependence on the cemenite lamellae orientation in a satisfactory way. The microcompression tests were performed at Erich Schmid Institute of Materials Science.

Acknowledgement

This work was performed in cooperation between the National Centre of Excellence CHARMEC (CHAlmers Railway MEChanics) and Erich Schmid Institute of Materials Science. Support from the industrial partner voestalpine Schienen GmbH is highly acknowledged. Furthermore, the simulations were performed on resources provided by the Swedish National Infrastructure for Computing (SNIC) at Chalmers Centre for Computational Science and Engineering (C3SE).

References

Allain, S., Bouaziz, O., 2008. Microstructure based modeling for the mechanical behavior of ferrite–pearlite steels suitable to capture isotropic and kinematic hardening. Mater. Sci. Eng. A 496 (1), 329–336.

Bažant, Z.P., 1986. Efficient numerical integration on the surface of a sphere. Z. für Angew. Math. Mech. 66 (1), 37–49.

Bouaziz, O., Le Corre, C., 2003. Flow stress and microstructure modelling of ferrite-pearlite steels during cold rolling. Mater. Sci. Forum 426–432 (2), 1399–1404.

Dafalias, Y.F., 2001. Orientation distribution function in non-affine rotations. J. Mech. Phys. Solids 49 (11), 2493–2516.

Hohenwarter, A., Taylor, A., Stock, R., Pippan, R., 2011. Effect of large shear deformations on the fracture behavior of a fully pearlitic steel. Metall. Mater. Trans. A 42, 1609–1618.

Hu, X., Van Houtte, P., Liebeherr, M., Walentek, A., Seefeldt, M., Vandekinderen, H., 2006. Modeling work hardening of pearlitic steels by phenomenological and Taylor-type micromechanical models. Acta Mater. 54 (4), 1029–1040.

Ivanisenko, Y., Lojkowski, W., Valiev, R., Fecht, H.-J., 2003. The mechanism of formation of nanostructure and dissolution of cementite in a pearlitic steel during high pressure torsion. Acta Mater. 51 (18), 5555–5570.

Johansson, G., Ekh, M., 2006. On the modeling of evolving anisotropy and large strains in pearlitic steel. Eur. J. Mechanics-A/Solids 25 (6), 1041–1060.

Kadkhodapour, J., Butz, a., Ziaei-Rad, S., Schmauder, S., 2011. A micro mechanical study on failure initiation of dual phase steels under tension using single crystal plasticity model. Int. J. Plast. 27 (7), 1103–1125.

Kapp, M.W., Hohenwarter, A., Wurster, S., Yang, B., Pippan, R., 2016. Anisotropic deformation characteristics of an ultrafine- and nanolamellar pearlitic steel. Acta Mater. 106, 239–248.

Larijani, N., Johansson, G., Ekh, M., 2013. Hybrid micro–macromechanical modeling of anisotropy evolution in pearlitic steel. Eur. J. Mechanics-A/Solids 38, 38–47.

Lindfeldt, E., Ekh, M., 2012. On the prediction of macroscopic yield surfaces for a pearlitic steel using computational homogenization. J. Multiscale Model. 4 (02).

March, A., 1932. Mathematische theorie der regelung nach der korngestalt bei affiner deformation. Z. für Kristallogr. 81, 285–297.

Menzel, A., Waffenschmidt, T., 2009 Sep 13. A microsphere-based remodelling formulation for anisotropic biological tissues. Philos. Trans. A Math. Phys. Eng. Sci. 367 (1902), 3499–3523.

Miehe, C., Schotte, J., 2004. Anisotropic finite elastoplastic analysis of shells: simulation of earing in deep-drawing of single-and polycrystalline sheets by Taylor-type micro-to-macro transitions. Comput. Methods Appl. Mech. Eng. 193 (1), 25–57.

Miehe, C., Schröder, J., Schotte, J., 1999. Computational homogenization analysis in finite plasticity Simulation of texture development in polycrystalline materials. Comput. Methods Appl. Mech. Eng. 171 (3–4), 387–418.

Peng, X., Fan, J., Yang, Y., 2002. A microstructure-based description for cyclic plasticity of pearlitic steel with experimental verification. Int. J. Solids Struct. 39 (2), 419–434.

Quey, R., Dawson, P., Barbe, F., 2011. Large-scale 3d random polycrystals for the finite element method: generation, meshing and remeshing. Comput. Methods Appl. Mech. Eng. 200 (1720), 1729–1745.

Raabe, D., Choi, P.P., Li, Y., Kostka, A., Sauvage, X., Lecouturier, F., Hono, K., Kirchheim, R., Pippan, R., Embury, D., 2010. Metallic composites processed via extreme deformation: toward the limits of strength in bulk materials. MRS Bull. 35 (12), 982–991.

Terada, K., Matsui, K., Akiyama, M., Kuboki, T., 2004. Numerical re-examination of the micro-scale mechanism of the bauschinger effect in carbon steels. Comput. Mater. Sci. 31 (1), 67–83.

Van Houtte, P., Li, S., Seefeldt, M., Delannay, L., 2005. Deformation texture prediction: from the Taylor model to the advanced Lamel model. Int. J. Plast. 21 (3), 589–624.

Watte, P., Van Houtte, P., Aernoudt, E., Sevillano, J., Van Raemdonck, W., Lefever, I., 1994. Work hardening of pearlite during wire drawing. Mater. Sci. Forum 157–6, 1689–1694.

Wetscher, F., 2006. Effect of Large Shear Deformation on Rail Steels and Pure Metals. Ph.D. thesis. University of Leoben.

Wetscher, F., Stock, R., Pippan, R., 2007. Changes in the mechanical properties of a pearlitic steel due to large shear deformation. Mater. Sci. Eng. A 445–446, 237–243.